

Nonlinear Interaction of Edge-Localized Modes and Turbulent Eddies in Toroidal Plasma under $n = 1$ Magnetic Perturbation

Jaehyun Lee,¹ Gunsu S. Yun,^{2,*} Minjun J. Choi,³ Jae-Min Kwon,³ Young-Mu Jeon,³ Woochang Lee,¹
Neville C. Luhmann, Jr.,⁴ and Hyeon K. Park^{1,3}

¹*Ulsan National Institute of Science and Technology, Ulsan 44919, Republic of Korea*

²*Pohang University of Science and Technology, Pohang 37673, Republic of Korea*

³*National Fusion Research Institute, Daejeon 34133, Republic of Korea*

⁴*University of California at Davis, Davis, California 95616, USA*

(Received 9 January 2016; published 8 August 2016)

The effect of static $n = 1$ resonant magnetic perturbation (RMP) on the spatial structure and temporal dynamics of edge-localized modes (ELMs) and edge turbulence in tokamak plasma has been investigated. Two-dimensional images measured by a millimeter-wave camera on the KSTAR tokamak revealed that the coherent filamentary modes (i.e., ELMs) are still present in the edge region when the usual large scale collapse of the edge confinement, i.e., the ELM crash, is completely suppressed by $n = 1$ RMP. Cross-correlation analyses on the 2D images show that (1) the RMP enhances turbulent fluctuations in the edge toward the ELM-crash-suppression phase, (2) the induced turbulence has a clear dispersion relation for wide ranges of wave number and frequency, and (3) the turbulence involves a net radially outward energy transport. Nonlinear interactions of the turbulent eddies with the coexisting ELMs are clearly observed by bispectral analysis, which implies that the exchange of energy between them may be the key to the prevention of large scale crashes.

DOI: 10.1103/PhysRevLett.117.075001

High confinement mode (H -mode) plasmas are characterized by an edge region with a steep pressure gradient and high current density called the pedestal and the semi-periodic collapse of the pedestal due to the development and crash of filamentary modes called edge-localized modes (ELMs) [1,2]. A reliable control of ELM crashes is an important issue for steady state burning plasma, because the heat and particle losses during the ELM crash are often spatially localized in the first surface causing damages on those hot spots. Perturbing the plasma edge by external magnetic fields is considered a promising solution to the ELM crash control via enhancement of particle transport and thereby reduction of the pressure gradient below the crash threshold [3]. In particular, resonant magnetic perturbation (RMP) has been applied successfully for suppression and/or mitigation of the ELM crashes in several tokamaks [4–7]. The Korea Superconducting Tokamak Advanced Research (KSTAR) device is equipped with a set of 12 coils at the outboard wall (4 top coils, 4 middle coils and 4 bottom coils). Each row of coils can produce a radial static magnetic field with toroidal mode number $n = 1$ or $n = 2$ depending on the coil current configuration [8]. It has been demonstrated experimentally that the RMP can suppress or mitigate the ELM crash without significant change of the energy confinement although neither the exact mechanism nor reliability of the control method is clear yet.

In the KSTAR device, the spatial structure and temporal dynamics of the ELM and edge turbulence have been

investigated in 2D using electron cyclotron emission imaging (ECEI) diagnostics [9,10]. It should be noted that the electron cyclotron emission (ECE) can be treated as a local measurement in the pedestal region even though the optical depth τ is marginal ($\tau \lesssim 1$) there. The high contrast and the coherent rotation of ELM filaments (Fig. 1) are good evidence of the localized measurement [11]. The ECE eventually becomes no longer localized close to and outside the separatrix (well known as shine-through problem), where the ECEI system cannot provide imaging.

The experiments for ELM-crash suppression were configured in a lower single null, high elongation $\kappa > 1.8$ and triangularity $\delta \approx 0.5$. The plasma current $I_p \approx 0.5$ MA, the magnetic field $B_0 \approx 1.9$ T, and the corresponding edge safety factor $q_{95} \approx 6$. Figure 1 shows the time history of the H_α signal and ECE images of distinctive ELM filaments at different stages of $n = 1$ RMP. The ELM has toroidal mode number $n \sim 15$ [12] and a pattern velocity of $v_{pt} \approx 1.7$ km/s along the electron diamagnetic direction before application of RMP. Note that the pattern velocity is the lab-frame velocity of the mode taking into account both the poloidal and toroidal plasma flow velocities (v_{pol} and v_{tor}):

$$v_{pt} = v_{pol} - v_{tor} \tan \alpha_* + v_{ph} = v_{\perp} / \cos \alpha_* + v_{ph}, \quad (1)$$

where α_* is the pitch angle near the midplane, v_{\perp} is the perpendicular plasma flow velocity, and v_{ph} is the phase velocity of mode in the plasma frame [13]. In the rising phase of the RMP current (I_{RMP}), the amplitude of the ELM

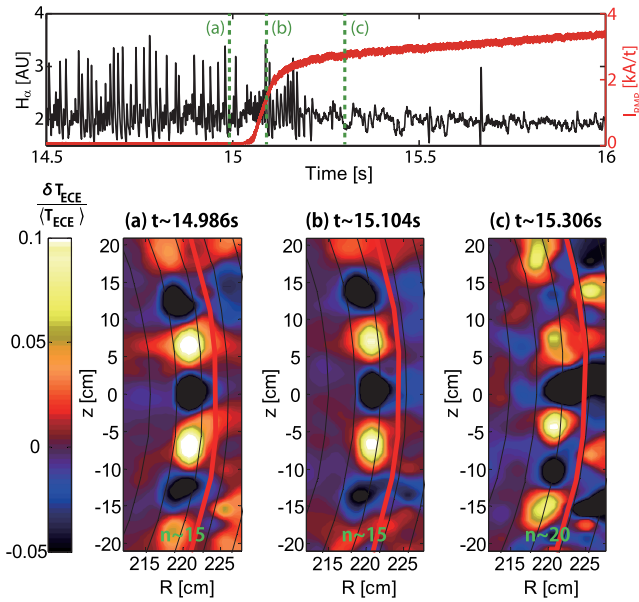


FIG. 1. Time history of H_α signal with RMP coil current I_{RMP} . ECE images of the pedestal region corresponding to (a) ELM structure in no. 10186 before application of RMP, (b) initial phase of RMP ramp-up, (c) ELM structure in the ELM-crash-suppression phase. Black lines are the reconstructed flux surfaces and the red line is the separatrix.

crash slightly reduced but the mode number ($n \sim 15$) remained the same.

Shortly after the ramp-up phase of I_{RMP} , ELM crashes were fully suppressed (i.e., no spikes in the H_α signal) but the filamentary ELMs still persisted at the edge with a higher mode number ($n \sim 20$) and more complex behavior compared to the ordinary ELMs with the usual quasiperiodic crashes (prior to the application of RMP): The filamentary mode appears and disappears repeatedly and sometimes bursts with small amplitude. The small burst events are easily identified by large spikes in the radio frequency (rf) signal of a filter-bank spectrometer similar to the case of the usual ELM crashes [14]. At the same time, the absence of H_α spikes at those burst events indicates that the bursts are localized in the plasma edge region, which is distinguished from the usual ELM crashes involving the collapse of the pedestal with large particle transport. The pattern velocity of the ELMs in the crash-suppression phase is typically small on the order of ~ 1 km/s and sometimes they appear to halt, similar to the reduction of perpendicular electron flow in the ELM-crash-suppression phase observed in DIII-D [15]. On the other hand, the pattern velocity of ordinary ELMs in the KSTAR device is observed in a wide range (up to several 10s km/s) in both electron and ion diamagnetic directions. As an important comparison, ELMs without bursts were also observed in some cases of ELM-crash suppression under RMP [Fig. 2(b)]. The absence of ELM bursts is supported by the quiescent RF signal. The mode grows and decays

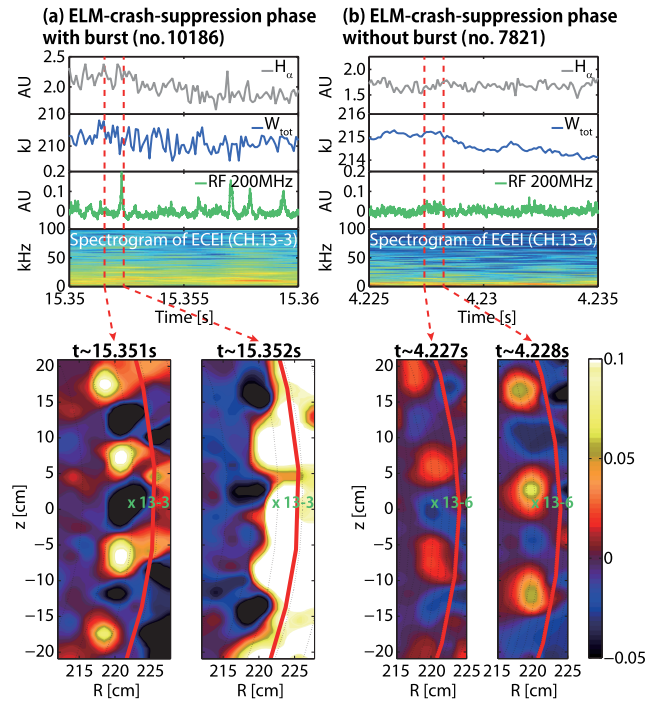


FIG. 2. Detailed time traces of H_α (lower divertor), stored energy, RF signal (200 MHz), and the ECEI spectrogram (the channel positions are indicated in lower ECE images) with respect to the existence of small bursts and corresponding ECE images: (a) ELM with small bursts (no. 10186) and (b) without bursts (no. 7821) during the ELM-crash-suppression phase. The red line in the ECE image is the separatrix position.

repeatedly in a random way. Assuming that the ELM filaments are formed along the magnetic field line, the lifetime of the nonbursting ELMs was estimated as $\sim 500 \mu\text{s}$, which is much shorter than the typical lifetime of ordinary ELMs, ~ 10 ms. These observations suggest that the RMP did not completely suppress the growth of ELMs but instead provided a damping to balance against the instability drive and thereby kept the perturbation amplitude below the threshold of a large ELM crash.

In an effort to understand the different dynamics among the three cases (ordinary ELMs, ELMs with small-scale bursts without pedestal collapse, and nonbursting ELMs), cross-correlation analyses including correlation coefficients, coherence, and cross-phase values among ECEI channels were performed to measure the wave dispersion of the turbulent fluctuations [16]. The cross-correlation analysis has been performed for a steady-state ELM-crash-suppressed H -mode plasma under the $n = 1$ RMP (time $t = 15.7 - 15.85$ s, line-average density $n_{e,l} \sim 2.5 \times 10^{19} \text{ m}^{-3}$, and toroidal velocity in the pedestal $v_{\text{tor,ped}} \sim 70$ km/s). Figure 3 is an example of coherence and cross-phase measurements for 4 (radial) \times 3 (poloidal) ECEI channels covering approximately $8 \times 5 \text{ cm}^2$ near $\psi \sim 0.95$, where ψ is the poloidal flux coordinate. The cross-correlation parameters are obtained at every 150 ms

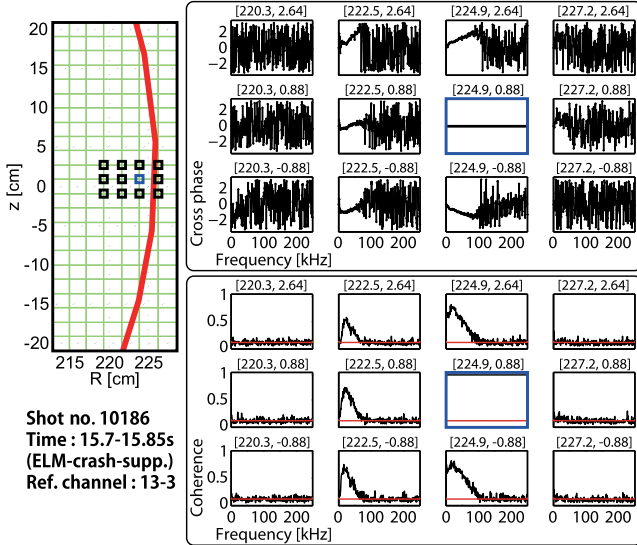


FIG. 3. The cross-phase and cross-coherence measurement using 4 (radial) \times 3 (poloidal) ECEI channels. Each channel position is marked by coordinates $[R, z]$. The red line is the separatrix position and the blue box indicates the reference channel for cross-correlation analysis. The red horizontal line in the cross-coherence plot is the statistical error limit.

by averaging over ten data segments of 15 ms duration (each segment contains 7,500 data points for 500 kHz sampling rate). This example clearly shows the existence of broadband and low frequency coherent modes ($f < 70$ kHz) along the poloidal direction in a narrow radial zone ($0.97 < \psi < 0.99$). Note that the random blackbody noise cannot make a substantial correlation among the channels well separated in space. The fact that the finite correlations were observed in the narrow radial zone along the specific poloidal direction suggests that the observations are real. Similar broadband fluctuations were also observed in magnetic signals by Mirnov coil array [8].

Two distinct features of the ELM-crash-suppressed phase identified by the correlation analysis are summarized in Fig. 4: (1) An ELM component around ~ 20 kHz and (2) broadband turbulent eddies. Note that the broadband turbulence structure has been observed in all cases of ELM-crash suppression regardless of the existence of the small localized bursts. The spectral power of the turbulence (30–70 kHz) increases with I_{RMP} while the spectral power of the ELM component (5–30 kHz) decreases [Fig. 4(a)]. This may suggest that the RMP induces the edge turbulence [17,18] and ELM crashes are suppressed when the edge turbulence level exceeds a certain threshold. The spectral power distribution $S_L(k_\theta, \omega)$ [19] in Fig. 4(b) shows the dispersion relation obtained from 2D ECEI signals in the ELM-crash-suppression phase. A clear dispersion relation is observed over a wide range of wave numbers ($k_\theta < 1$ cm $^{-1}$) and frequency ($f < 70$ kHz) with the average group velocity ~ 3 km/s along the electron diamagnetic direction in the laboratory frame. Note that the dispersion

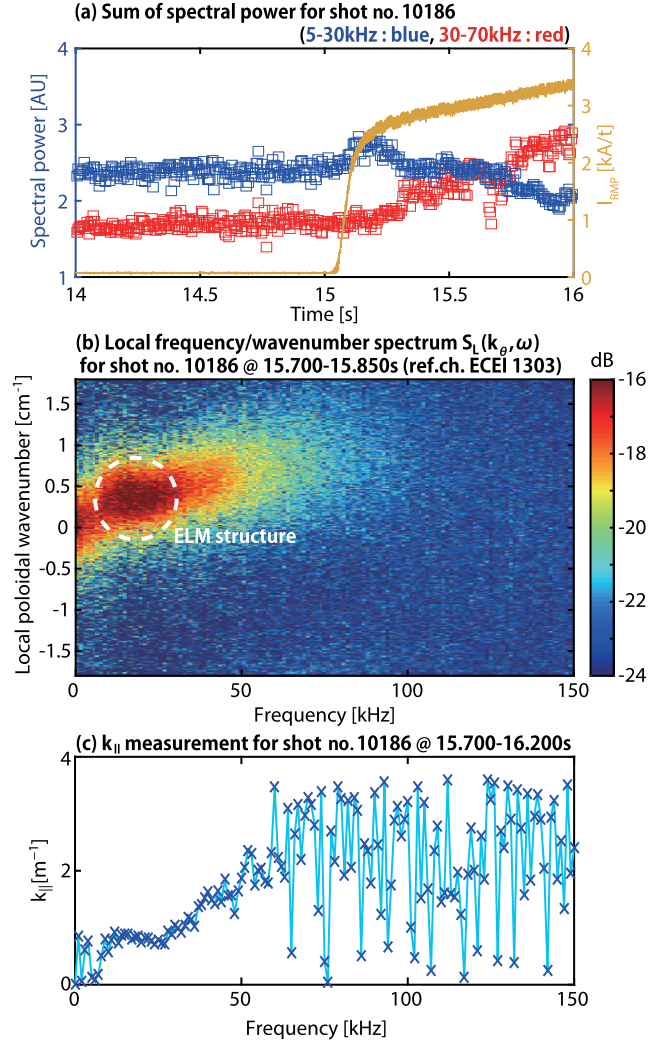


FIG. 4. (a) The time traces of integrated spectral powers of ELM (blue; 5–30 kHz) and turbulence (red; 30–70 kHz) along with the RMP coil current. (b) The spectral power distribution $S_L(k_\theta, \omega)$ in the ELM-crash-suppression phase. (c) Parallel wave number measurement using two toroidally separated ECE imaging systems.

curves in both Figs. 4(b) and 4(c) change the slope slightly around the ELM frequency. The measured wave number allows one to deduce the characteristic size of the turbulence, usually compared with the hybrid Larmor radius $\rho_s = \sqrt{2m_i T_e}/eB$ where m_i is the ion mass and e is the electric charge. In this example case, $k_\theta \rho_s < 0.1$ using $\rho_s \sim 1$ mm at the edge. Kinetic ballooning modes (KBMs) [20], microtearing modes (MTMs) [21], resistive ballooning modes (RBMs) [22], and ion temperature gradient (ITG) modes [23] are of similar size ($k_\theta \rho_s \sim 0.1$ in a tokamak). These instability modes can be distinguished by the propagation direction: KBM and ITG propagate in the ion diamagnetic direction, the MTM propagates in the electron diamagnetic direction, and the RBM does not have any preferential direction. The observed group velocity of

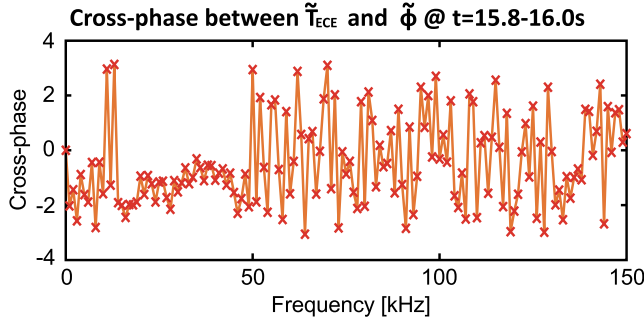


FIG. 5. Cross-phase analysis between \tilde{T}_{ECE} and $\tilde{\phi}$ during the ELM-crash suppression phase.

the turbulence suggests the plasma frame phase velocity of the turbulence (v_{ph}) is in the electron diamagnetic drift direction since the expected poloidal flows cannot exceed the sum of other factors in the KSTAR plasma, i.e., $|v_{\text{pol}}| < |v_{\text{pt}} + v_{\text{tor}} \times \tan \alpha_*| \approx 12$ km/s. Figure 4(c) is the dispersion of the parallel wave number k_{\parallel} during the ELM-crash-suppression phase measured by the two independent ECEI systems [10] separated by 1/16th of the torus circumference on the KSTAR device. A broad dispersion is found for $f < 70$ kHz and $10/qR < k_{\parallel} < 20/qR$, where $q \approx 6$ is the safety factor at the mode position $R \approx 2.25$ m. k_{\parallel} is determined by measuring the phase delay $\Delta\Phi_{12}$ between the two systems according to the relation, $k_{\parallel} = \Delta\Phi_{12}/\Delta l$, where Δl is the distance between the two toroidally separated view positions.

The effect of the turbulent eddies on the radial transport can be studied by measuring the phase relationship between the radial velocity fluctuations (\tilde{v}_r) and the ECE intensity fluctuations (\tilde{T}_{ECE}). Because $\tilde{T}_{\text{ECE}}/T_{\text{ECE}} = (1 + A_2)\tilde{T}_e/T_e + A_2\tilde{n}_e/n_e$ in the edge region where $0 < A_2 < 1$ is a numerical function of the optical depth and wall reflection [24,25], the radial flux $\Gamma_{\text{ECE}} = \frac{1}{2}\langle \tilde{v}_r \tilde{T}_{\text{ECE}} \rangle$ may be considered as a combination of particle and heat flux. The cross-correlation velocimetry technique with time-delay estimation [26] is applied to the ECE images to track the high speed motion of the turbulent eddies which are moving and deforming in the presence of the turbulent flow field and then obtain \tilde{v}_r . The measured cross-phase value between \tilde{v}_r and \tilde{T}_{ECE} during the ELM-crash suppression period is approximately zero in the range of 30–50 kHz, suggesting that the turbulent eddies cause a net outward energy flux $\Gamma_{\text{ECE}} \propto |\tilde{T}_{\text{ECE}}|^2 > 0$. This is consistent with the observed reduction of the stored energy (by about 10%–30%) [8] and may have prevented the buildup of free energy for the ELM growth. Note that the velocimetry analysis also provides the information on the potential fluctuations $\tilde{\phi}$ (Fig. 5) assuming the relation $\tilde{v}_r = \tilde{E}_{\theta}/B = -\nabla_{\theta}\tilde{\phi}/B = -ik_{\theta}\tilde{\phi}/B$ (here, \tilde{E}_{θ} is the poloidal electric field component) [27]. If independent simultaneous measurement of \tilde{n}_e is available, the cross-phase measurement between $\tilde{\phi}$ and \tilde{n}_e can be used to distinguish

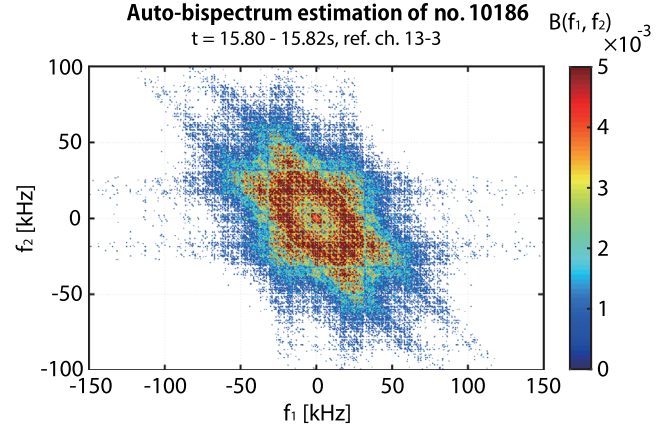


FIG. 6. Auto-bispectrum of a single ECEI channel in the ELM-crash-suppression phase.

among different instability drives (e.g., $\pi/2$ for the interchange mode and 0 for the drift mode [28]).

In addition to the particle flux enhancement by the turbulent eddies in the ELM-crash-suppression phase, nonlinear interactions are expected between ELMs and turbulent eddies as they coexist in the $S_L(k_{\theta}, \omega)$ plot [Fig. 4(b)]. The simplest nonlinear interactions are the three-wave coupling represented by the bispectrum $B(f_1, f_2) = F(f_1)F(f_2)F^*(f_1 + f_2)$ where F denotes the Fourier transform and f 's denote the wave frequencies [29]. As expected from nonlinear interactions between a narrow-band coherent wave (i.e., ELM with frequency f_{ELM}) and broadband waves (i.e., turbulent eddies), the auto-bispectrum plot obtained from ECEI signals (Fig. 6) shows line features (vertical, horizontal, and -45° lines with intercepts at $\pm f_{\text{ELM}}$). Note that these lines are essentially identical by the symmetries of bispectrum $B(f_{\text{ELM}}, f) = B(f, f_{\text{ELM}}) = B^*(f_{\text{ELM}} + f, -f) = B(-f_{\text{ELM}} - f, f)$. No such line features are observed in the bispectrum of ECEI signals before the suppression of ELM crashes. The nonlinear interaction revealed by the bispectrum (Fig. 6) and the opposite trends in the spectral power between ELM and turbulent eddies [Fig. 4(a)] suggest that the turbulent fluctuations induced by RMP dissipate the free energy for the ELM growth.

In summary, the ELM-crash-suppression phase under $n = 1$ RMP is characterized by the coexistence of the filamentary ELMs and smaller scale turbulent eddies in the edge. It is found that the filamentary structure of ELMs is maintained with substantial fluctuations in amplitude without large scale collapse, which is distinguished from the ordinary ELMs with a quasiperiodic collapse of the pedestal. The cross-correlation technique on the 2D ECEI signals revealed that the turbulence at the edge has a wide range of poloidal wave numbers $k_{\theta} < 1$ cm^{-1} and rotates in the electron diamagnetic direction with a parallel wave number in the range of $10/qR < k_{\parallel} < 20/qR$. The radial velocity and ECE intensity fluctuations of these turbulent eddies are approximately in phase and thus the turbulence involves a net radial energy

transport. The bispectrum analysis clearly shows that the coexisting ELMs and turbulent eddies nonlinearly interact with each other. However, it is not clear whether the nonlinear interaction suppresses the ELM growth and/or facilitates the triggering of the small-scale burst, which remains to be studied in the future. Both the enhancement of radially outward transport and the nonlinear interaction with ELMs are the main effects of the edge turbulence and may be the key to the physics mechanism of ELM-crash suppression by low- n RMP.

The authors thank Dr. Steve Sabbagh and Dr. Young-seok Park for providing equilibrium reconstruction, Dr. Sandor for helping correlation analyses, the POSTECH, UNIST, and KSTAR teams for supporting the operation of the ECEI and fast RF spectrometer systems. This work was supported by National Research Foundation of Korea under Grants No. 2014M1A7A1A03029865, No. 2014M1A7AA03029881, the BK21+ program and by the U.S. DOE under Contract No. DE-FG02-99ER54531.

*Corresponding author.
gunsu@postech.edu

- [1] J. W. Connor, Edge-localized modes – physics and theory, *Plasma Phys. Controlled Fusion* **40**, 531 (1998).
- [2] W. Suttrop, The physics of large and small edge localized modes, *Plasma Phys. Controlled Fusion* **42**, A1 (2000).
- [3] T. E. Evans, R. A. Moyer, and P. Monat, Modeling of stochastic magnetic flux loss from the edge of a poloidally diverted tokamak, *Phys. Plasmas* **9**, 4957 (2002).
- [4] T. E. Evans *et al.*, Suppression of Large Edge-Localized Modes in High-Confinement DIII-D Plasmas with a Stochastic Magnetic Boundary, *Phys. Rev. Lett.* **92**, 235003 (2004).
- [5] Y. Liang *et al.*, Active Control of Type-I Edge-Localized Modes with $n = 1$ Perturbation Fields in the JET Tokamak, *Phys. Rev. Lett.* **98**, 265004 (2007).
- [6] A. Kirk *et al.*, Resonant magnetic perturbation experiments on MAST using external and internal coils for ELM control, *Nucl. Fusion* **50**, 034008 (2010).
- [7] W. Suttrop *et al.*, First Observation of Edge Localized Modes Mitigation with Resonant and Nonresonant Magnetic Perturbations in ASDEX Upgrade, *Phys. Rev. Lett.* **106**, 225004 (2011).
- [8] Y. M. Jeon *et al.*, Suppression of Edge Localized Modes in High-Confinement KSTAR Plasmas by Nonaxisymmetric Magnetic Perturbations, *Phys. Rev. Lett.* **109**, 035004 (2012).
- [9] G. S. Yun *et al.*, Development of KSTAR ECE imaging system for measurement of temperature fluctuations and edge density fluctuations, *Rev. Sci. Instrum.* **81**, 10D930 (2010).
- [10] G. S. Yun *et al.*, Quasi 3D ECE imaging system for study of MHD instabilities in KSTAR, *Rev. Sci. Instrum.* **85**, 11D820 (2014).
- [11] G. S. Yun, M. J. Choi, W. Lee, H. K. Park, C. W. Domier, and N. C. Luhmann Jr., High contrast 2D visualization of edge plasma instabilities by ECE imaging, *J. Instrum.* **7**, C01024 (2012).
- [12] J. Lee *et al.*, Toroidal mode number estimation of the edge-localized modes using the KSTAR 3-D electron cyclotron emission imaging system, *Rev. Sci. Instrum.* **85**, 063505 (2014).
- [13] G. S. Yun *et al.*, Two-dimensional imaging of edge-localized modes in KSTAR plasmas unperturbed and perturbed by $n = 1$ external magnetic fields, *Phys. Plasmas* **19**, 056114 (2012).
- [14] J. Leem, G. S. Yun, and H. K. Park, Development of fast RF spectrometer system for MHD detection, *J. Instrum.* **7**, C01042 (2012).
- [15] R. Nazikian *et al.*, Pedestal Bifurcation and Resonant Field Penetration at the Threshold of Edge-Localized Mode Suppression in the DIII-D Tokamak, *Phys. Rev. Lett.* **114**, 105002 (2015).
- [16] B. H. Deng, D. L. Brower, G. Cima, C. W. Domier, N. C. Luhmann Jr, and C. Watts, Mode structure of turbulent electron temperature fluctuations in the Texas Experimental Tokamak Upgrade, *Phys. Plasmas* **5**, 4117 (1998).
- [17] J. D. Callen, Pedestal structure without and with 3D Fields, *Contrib. Plasma Phys.* **54**, 484 (2014).
- [18] G. D. Conway, S. Fietz, H. W. Müller, T. Lunt, P. Simon, W. Suttrop, M. Maraschek, T. Happel, and E. Viezzer, Impact of magnetic perturbation coils on the edge radial electric field and turbulence in ASDEX Upgrade, *Plasma Phys. Controlled Fusion* **57**, 014035 (2015).
- [19] J. M. Beall, Y. C. Kim, and E. J. Powers, Estimation of wavenumber and frequency spectra using fixed probe pairs, *J. Appl. Phys.* **53**, 3933 (1982).
- [20] Z. Yan, G. R. McKee, R. J. Groebner, P. B. Snyder, T. H. Osborne, M. N. Beurskens, and K. H. Burrell, Pedestal density fluctuation dynamics during the inter-ELM cycle in DIII-D, *Phys. Plasmas* **18**, 056117 (2011).
- [21] D. Told, F. Jenko, P. Xanthopoulos, L. D. Horton, and E. Wolfrum, Gyrokinetic microinstabilities in ASDEX Upgrade edge plasmas, *Phys. Plasmas* **15**, 102306 (2008).
- [22] C. Bourdelle, X. Garbet, R. Singh, and J. Schmitz, New glance at resistive ballooning modes at the edge of tokamak plasmas, *Plasma Phys. Controlled Fusion* **54**, 115003 (2012).
- [23] G. S. Lee and P. H. Diamond, Theory of ion-temperature-gradient-driven turbulence in tokamaks, *Phys. Fluids* **29**, 3291 (1986).
- [24] C. Janicki, Electron temperature measurement from the ECE diagnostics in tokamak plasmas under transient conditions, *Nucl. Fusion* **33**, 513 (1993).
- [25] S. J. Zweben, J. A. Boedo, O. Grulke, C. Hidalgo, B. LaBombard, R. J. Maqueda, P. Scarin, and J. L. Terry, Edge turbulence measurements in toroidal fusion devices, *Plasma Phys. Controlled Fusion* **49**, S1 (2007).
- [26] T. Munsat and S. J. Zweben, Derivation of time-dependent two-dimensional velocity field maps for plasma turbulence studies, *Rev. Sci. Instrum.* **77**, 103501 (2006).
- [27] P. Manz, J. E. Boom, E. Wolfrum, G. Birkenmeier, I. G. J. Classen, N. C. Luhmann, and U. Stroth, Velocimetry analysis of type-I edge localized mode precursors in ASDEX Upgrade, *Plasma Phys. Controlled Fusion* **56**, 035010 (2014).
- [28] B. D. Scott, Drift wave versus interchange turbulence in tokamak geometry: Linear versus nonlinear mode structure, *Phys. Plasmas* **12**, 062314 (2005).
- [29] Y. C. Kim, J. M. Beall, E. J. Powers, and R. W. Mksad, Bispectrum and nonlinear wave coupling, *Phys. Fluids* **23**, 258 (1980).